
Article:
Sherriff, M. orcid.org/0000-0003-3212-6233, Griffo, A. orcid.org/0000-0001-5642-2921, Jia, C. et al. (3 more authors) (2025) Partial discharge in silicone gel on power module substrates in high-humidity conditions. IEEE Transactions on Dielectrics and Electrical Insulation, 32 (1). pp. 484-493. ISSN 1070-9878

https://doi.org/10.1109/tdei.2024.3404367

Partial Discharge in Silicone Gel on Power Module Substrates in High-Humidity Conditions

Mark Sherriff, *Student member, IEEE* Antonio Griffo, *Member, IEEE*, Chunjiang Jia, Chong Ng, Zi-Qiang Zhu, *Fellow, IEEE*, and David A. Stone

***Abstract*— Partial discharge (PD) is known to affect quality of insulation in power electronics modules. This paper provides a comprehensive characterisation of PD activity in gel-encapsulated direct bonded copper (DBC) power module substrates when subjected to fast unipolar square excitations. PD characteristics in low and high humidity environments are compared. PD inception voltage (PDIV) testing and time-resolved PD (TRPD) analysis is performed to investigate discharges in each condition. Two PD groups are identified, categorised by their amplitude, and prompting further investigation of the weaker group with a statistics-based approach. The strong group does not vary with humidity and is attributed to discharges between the top and bottom copper of the DBC. The weaker group varies significantly with humidity and is attributed to discharges within the lateral trench gap of the DBC top copper.**

***Index Terms*— Harsh Environment, Reliability, Partial Discharge, Power modules.**

I. Introduction

PARTIAL discharge (PD) ruggedness of high voltage power modules is critical for reliable operation in harsh environments, resulting in fewer failures and consequently reducing maintenance and repair costs. Power converters in offshore energy generation, aerospace and automotive applications are subjected to many environmental stressors including high temperatures, high ambient humidity and contamination [1]–[3]. Increasing energy demand and growing consumer bases also push these sectors towards increasing operating voltages and system miniaturization. Power devices based on Silicon (Si) and more recently on Silicon Carbide (SiC) and Gallium Nitride (GaN) [4]–[6], are usually packaged in modules using similar encapsulation materials, typically based on silicone gels and substrates and are subsequently limited by the same packaging-related reliability concerns. Macroclimate approaches towards reducing hazardous environments within control cabinets can prove effective in some cases [7], but cost and volume constraints limit their feasibility.

Early studies on the PD behaviours of silicone gel were performed in 2006 [8], concluding that increasing temperature had little impact on the PD inception voltage (PDIV). This disagreed with contemporary research for solid insulation such as high-voltage cabling in [9], or insulated stator bars in [10], which showed that PD activity was exacerbated or PDIV reduced with increasing temperature. Around that time, studies investigated the breakdown characteristics of silicone gel thoroughly under various conditions [11], [12], concluding that proper degassing of the material can help eliminate the presence of voids within the gel or at interfaces and reduce the quantity of uncured silicone fluid, both of which generally increased the breakdown strength under 50 Hz AC stimulus. Later, ceramic substrates were incorporated in testing, showing that for silicone gel insulation the PDIV was not impacted in a significant manner by increasing temperature [13]. However, this study revealed that the absolute number of PD events was greatly increased with increasing temperature. Additionally, the authors here reasoned that the PDs occurred within the substrate itself, and not the gel. Though a 2007 study highlighted the severe reduction in insulation quality of silicone gel in high humidity [14], the picture is not clear when considering combined temperature and humidity stress for solid insulation. An earlier study on enamelled magnet wires showed that increasing ambient humidity at low temperatures (30 °C) reduced PDIV but had little impact at higher temperatures (≥ 60 °C) [15]. The same authors found a strong dependence on temperature in the humidity-driven change of PDIV on similar samples with PD measured by optical emission spectroscopy in 2010 [16] and investigate the combined impact in [17]. More recently it was shown that increasing temperature served generally to reduce PDIV, especially at lower ambient humidity, for solid insulation [18]. This is somewhat in disagreement with the later results of [19] that the impact of temperature and humidity on the PD characteristics of solid insulation is strongly nonlinear. The variation could be due to the test stimulus applied, as the former utilised surge voltage for PDIV measurement, while the latter used 50 Hz AC.

The authors of [20] thermally aged silicone gel encapsulated direct bonded copper (DBC) substrate samples in high and low humidity environments. The latter had little bearing on the PD and breakdown behaviours, but the former showed a multifaceted impact: PDIV was generally increased, but the variation was significantly increased. The authors observe the same reduction in breakdown voltage for the humid-aged samples as reported by the previous work in [14], and comment on the inability of contemporary standard IEC 61287:2006 to stress the substrate in a fully representative manner. The recent version of this standard and other relevant current standards do not ameliorate this issue [21]–[23].

There is uncertainty regarding geometric and material variations to power module designs to increase PD ruggedness, and these approaches are not yet mature for field operation. PD behaviours have shown a complex nonlinear relationship with temperature and humidity for gel encapsulation which is not yet

fully understood. The test waveform is also a highly sensitive parameter, and the test configuration of current standards is not sufficient to stress substrates fully. Consequently, there is a need to test real field operating substrates in representative environmental conditions, with test stimuli representative of field operation.

This paper provides a comprehensive experimental investigation aimed at characterising and quantifying PD activity in DBC samples from commercial power modules when subjected to fast repetitive voltage impulses. PD characteristics in harsh environments with low and high ambient humidity are compared. PDIV, PD count, PD intensity and PD time lag are quantified and correlated to the two environmental conditions in an extensive set of experiments. Two groups of PD behaviours are identified, categorised by discharge amplitude. Further investigation with a statistics-based approach revealed that the weaker group was highly susceptible to variation in PD count with changes in ambient humidity. This weaker group is attributed to discharges within the silicone gel or at the triple junction in the trenches between top copper potions of the DBC. The stronger group did not vary in nature with humidity and is attributed to discharges within the ceramic between the top and bottom copper of the DBC.

II. Sample Detail and Experiment Setup

A. Sample Preparation

Individual DBC rafts were harvested from IGBT half bridge modules (Infineon FF100R17IE4) for testing, allowing for test samples representative of those used in field operation. The IGBT housing was first removed, and the busbars cut off carefully. Then most of the original silicone gel was manually removed using plastic tools to ensure the copper surface was not damaged. Bond wires were then removed so that the baseplate could be placed on a hot plate and the DBC rafts desoldered. The IGBT and diode dies were similarly desoldered from the individual rafts, leaving only the DBC substrate behind.

A thorough repeat cleaning procedure using IPA solution, fine-bristled brushes and fine abrasion was then performed on each sample to remove residual silicone gel and remaining surface solder. Removal of the gel was verified with scanning electron microscope (SEM) imaging and energy-dispersive x-ray spectroscopy (EDS). EDS mapping is an imaging technique in which a high energy electron beam is used to generate characteristic x-rays from target materials, which are used to determine the elemental content. An example of this is shown in Fig. 1. Chemical solutions such as toluene, methylated spirits (denatured alcohol), or targeted silicone gel removers were not used as they would degrade the surface copper of the DBC as shown in [24]. Once clean and dry, cross-linked polyethylene (XLPE) insulated leads were soldered to the rafts, and the edge and back copper were bonded using silver paste (Electrodag 1415) to achieve the final test geometry. This configuration allowed for stressing of both the lateral trench and the ceramic in the vertical direction, as suggested by [20]. The rafts were then affixed into ABS potting boxes with cyanoacrylate (CA)

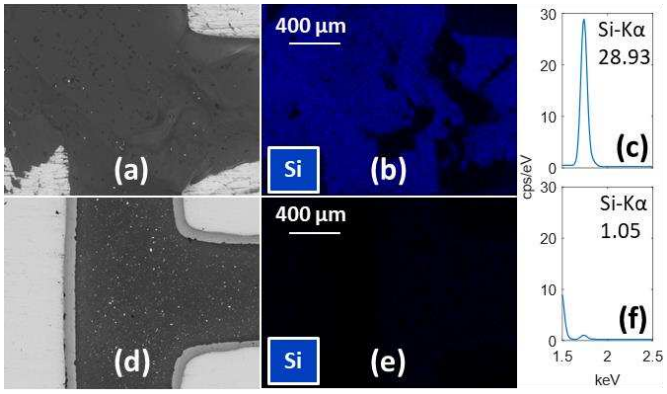

Fig. 1. SEM and EDS images of Si distribution on a section of a sample before and after cleaning. (a) SEM before, (b) EDS before, (c) Si-Kα before, (d) SEM after, (e) EDS after, and (f) Si-Kα after.

glue, and new silicone gel was poured over top, to a depth of 3 mm. The gel used was Wacker SilGel 612, a two-component room temperature vulcanising (RTV) silicone rubber. The dielectric strength of this gel exceeds 23 kV/mm. In line with manufacturer processing guidelines, the gel was first mixed in clean glassware and then degassed under vacuum (approximately 30 mBar) for no longer than 10 minutes. The gel was then poured into the sample moulds in two stages before being degassed again at each stage. Samples were then placed in a controlled environment of 85 °C, 30% RH and normal ambient pressure to cure for at least 8 hours. Once cured, samples were allowed to cool before being subjected to insulation resistance testing to rule out any early failures. A total of 5 DBC rafts were qualified to be used in testing. A photograph of a sample is provided in Fig. 2.

B. Test Platform

A bespoke PD testing setup was designed and built for this research. A circuit diagram of the major components is shown in Fig. 3. A SiC MOSFET push-pull switch from Behlke Power Electronics (HTS 81-15-SiC-GSM) was used with a high voltage (HV) DC supply (Glassman EQ, 20 kV) to provide test voltage pulses to the samples. The switch and power supply are user configurable, controlled by a National Instruments (NI) Compact RIO (cRIO) 9063. As the output of the HVDC supply is limited to only 60 mA, a 68 nF boost capacitor was connected in parallel to the HV output and charged prior to testing. A 680 Ω power resistor was used to limit overshoot of the test pulses. Test samples were placed within an environment chamber (Espec SH-662) for the duration of testing. A HV differential probe (Pico Technology TA044) was used to measure the test pulses. A labelled photograph of the control cabinet is provided in Fig. 4. Most PD detection setups are based on the international standard IEC 60270, which provides guidelines for retrieval of PDIV, PD extinction voltage (PDEV) and the corresponding apparent charge of PD events [22]. Generally, this standard focuses on AC testing of samples, or with fixed DC voltage. The more applicable standard for switching scenarios is IEC 61934, which provides guidelines for

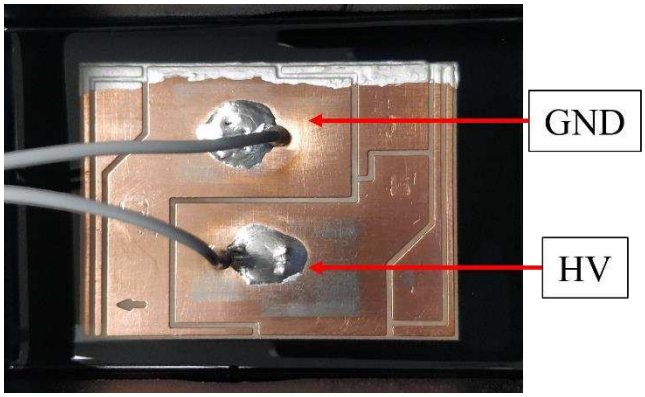

Fig. 2. Photograph of encapsulated DBC sample used in testing.

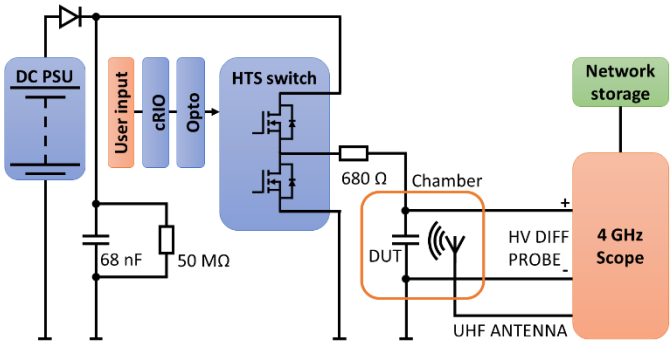

Fig. 3. Diagram of major components of bespoke PD testing platform.

measurements under repetitive impulses with fast rise times [23]. A PD detection method put forth in this standard is measurement of the ensuant electromagnetic interference (EMI) caused by a PD event within a sample. This is measured by ultra-wideband (UWB) antennas, usually sensitive to the ultra-high frequency (UHF) range of 0.3–3 GHz.

To measure radiated emissions from the test samples, a potted monopole antenna manufactured by Schleich GmbH was used. Though this Schleich potted monopole antenna (SPMA) was used as a basis for comparison previously in [25], additional validation for this work was performed by comparison of PD detection ability with a wideband log periodic antenna (LPA). This revealed that the UHF sensitivity of the SPMA was sufficient to provide the appropriate sensitivity to PD EMI, being in every case as sensitive or more so than the LPA to the observed discharges. The potted construction of the antenna guards against harmful humidity ingress and allows it to be placed within the environment chamber close to test samples. SPMA position inside the chamber was determined by experiment to have negligible impact on measured signal strength.

Pulses with fast voltage gradients of up to 23 kV/µs are generated by the equipment, generating considerable high-frequency EMI. Consequently, and in line with IEC 61934, high pass filtering for PD detection was required. A 7th-order Butterworth high-pass filter (HPF) from Crystek (CHPFL-0700) with a cut-off frequency of 700 MHz was used and provided sufficient distinction between commutation EMI and

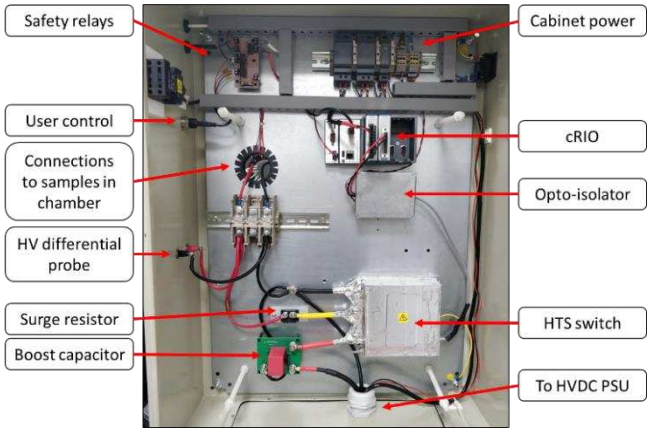

Fig. 4. Labelled photograph of control cabinet of PD test platform.

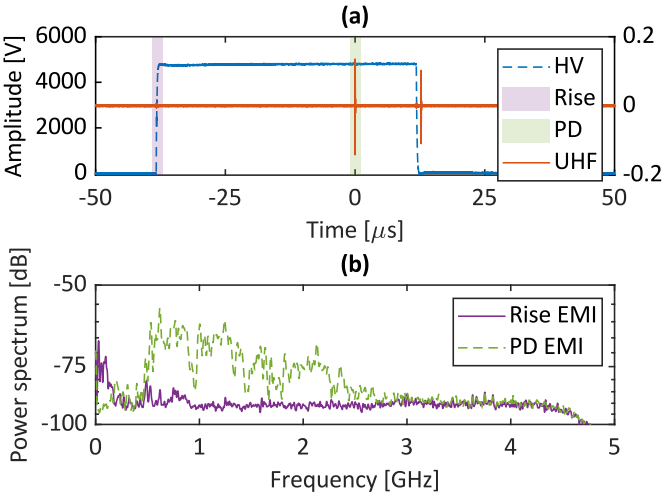

Fig. 5. Typical characteristics of PD generated by a HV square pulse. (a) time domain, and (b) spectra.

PD EMI for high amplitude discharges. The sample rate used in these experiments was 10 GS/s. Fig. 5 shows typical time domain behaviours and filtered radiated emissions from the samples when no PD was detected and when PD was observed for a 4.8 kV test with 50 µs square pulse width. The no-PD event was recorded during the rise of the test pulse, and the PD event was observed during the test voltage high plateau, when no other excitations were present. The no-PD spectrum is then considered to be related purely to the commutation of the test voltage and has frequency content up to 900 MHz. The PD event spectrum overlaps the commutation spectrum between 450–900 MHz, but also has significant high frequency content up to 2.5 GHz. Consequently, this setup was determined to be sufficient for the detection of PD. These spectra were consistently observed in many repetitions of similar experiments with only slight variations. The system was tested to be free of PD under open configuration.

C. PDIV Determination Test Procedure

An in-situ photograph of the test setup is provided in Fig. 6. Samples were placed inside the environment chamber and raised from the metal racking with polypropylene (PP) spacers.

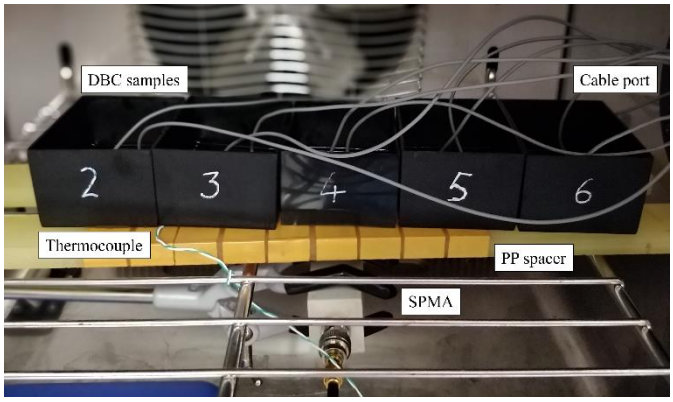

Fig. 6. Samples in environment chamber with antenna placed below. Each numbered pot (2–6) contains a single sample, an example of which is shown in Fig. 2.

The antenna was placed on the bottom of the chamber, raised to be close to the samples. The soldered XLPE-insulated leads were fed through the foam cable port, which was then sealed, providing exterior connection to test stimulus for each sample in turn via insulated spade connectors. The antenna was connected to the oscilloscope using RG316 coaxial cable, which was fed through the chamber door seal, to avoid proximity to the sample connections. Care was taken to separate the cabling to avoid potential PD between conductors, rather than inside the samples.

Samples placed within the environment chamber were initially held in a dry-out condition (85 °C, 30% RH) for 24 hours before testing, to drive off any absorbed moisture while in storage. This work makes comparison of the sample PD characteristics in low-humidity conditions (85 °C / 30% RH) and high-humidity conditions (85 °C / 85% RH). The temperature used for each condition was the same to eliminate the influence of temperature on the results. Test conditions are summarized in Table I.

Samples were held at each condition for 24 hours before testing to ensure that any absorption activity had ceased. Samples were individually subjected to 5 periods of a 10 kHz 50% duty cycle square wave for the purposes of generating PD. Multiple impulses at a given test voltage are used to combat the stochastic nature of PD. After each pulse train the HVDC supply was increased by a 50 V increment, with a step delay time of 1 s to charge the boost capacitor. The test voltage started at 1 kV based on prior experience with similar samples, and ceased when PD was detected based on a 100 mV trigger on the UHF antenna reading. Though standards indicate that a threshold of twice the noise floor (~25 mVpp, based on residual commutation EMI) is sufficient, intermittent external noise

TABLE I
SUMMARY OF TEST CONDITIONS

Condition	Temp. [°C]	Humidity [% RH]	Step time [h]	Test time [h]
1: RH30-24h	85	30	24	24
2: RH85-24h	85	85	24	48
3: RH85-48h	85	85	24	72
4: RH30-24h	85	30	24	96

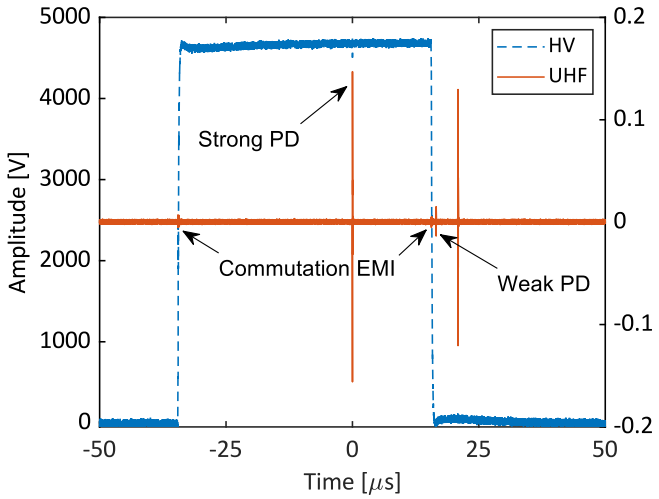

Fig. 7. Typical PDIV test with HV (dashed) and UHF (solid) shown.

sources required an elevated threshold. Testing was repeated a total of 5 times for each sample in each condition. A single switching event of a representative test case is shown in Fig. 7, where two distinct strengths of PD can be identified.

D. Weak PD Count Procedure

The two strengths of PD were witnessed several times during testing: These groups are termed strong and weak PD based on their amplitudes. Weak PD exhibited similar power spectra to the residual commutation EMI and could occur at the commutation intervals. Consequently, proper detection of the weak PD was not trivial.

As weak PD also exhibited a low probability of occurrence, testing was performed using single pulses at fixed voltages in steps of 100 V from 3500–4000 V, with 100 tests at each voltage. To allow for settling of space charges and to save the data, a delay of 4 s was added between each test. The environment chamber does not fully isolate the antenna from outside noise sources, so steep software band stop filters were applied to the recorded UHF data to increase the signal-to-noise ratio. Care was taken with the cut-off frequencies of the band pass filters as several external noise sources overlapped PD in the frequency domain. Their attenuation bands were as follows: 725–945 MHz, 1680–1790 MHz, 2385–2500 MHz.

The rest of the post processing followed the approach of [26] with some modifications. Individual PD events were counted based on a 100 ns window, where samples within that window were considered to arise from the same PD event. This window was chosen empirically. The moving standard deviation was chosen to better highlight PD activity from the background noise, and the alignment was used to cope with pulse width jitter caused by the pulse generator. Samples were held at the dry-out condition for 24 h before testing. Due to the large quantity of tests at a given condition only high and low humidity conditions were inspected after a 24 h dwell time, commensurate with the first 2 test conditions in the previous test. Categorisation of strong and weak PD in this work used an amplitude of above or below 100 mVpp, respectively.

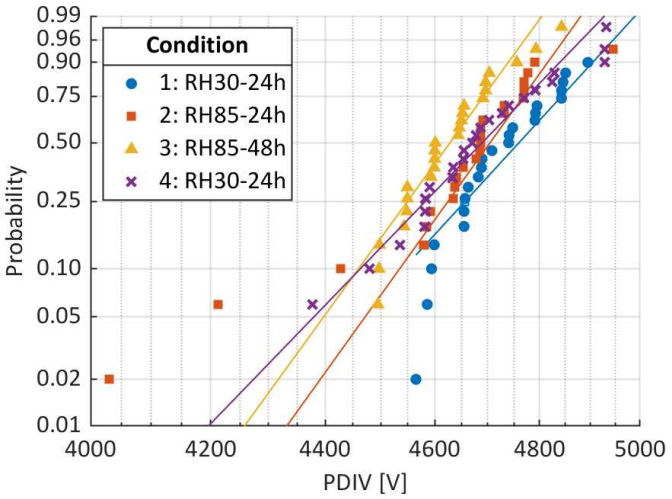

Fig. 8. Two-parameter Weibull distribution plots of PDIV tests for strong PD at each subsequent environmental condition: 1: 30% RH / 24 h (●); 2: 85% RH / 24 h (■); 3: 85% RH / 48 h (▲); 4: 30% RH / 24 h (×).

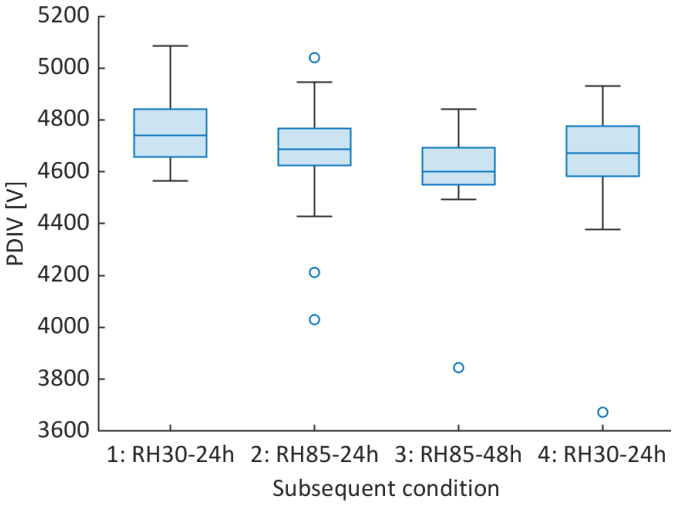

Fig. 9. Box chart of PDIV tests at each subsequent condition. Conditions are outlined in Table I.

III. Effect of Humidity on PD Activity

A. PDIV Determination Testing

In this work, PDIV was determined to be the voltage during the square pulse plateau region in a test which demonstrates strong PD. This was used to simplify the view of the results considering the fast rise times of the pulse and its oscillatory behaviour, as well as the presence of PD after the falling edge. Relevant standards indicate that a threshold of twice the noise floor is sufficient for PD detection using UHF sensors, but the residual commutation EMI after hardware filtering was enough to exceed this threshold. Consequently, and based on previous experimentation, the threshold for triggering the oscilloscope and hence identifying that PD had occurred was set to 100 mV. This threshold was sufficient to ensure that strong PD was the focus of this test.

The two-parameter Weibull distribution is used to show the PDIV results for all tested samples at each environmental condition in Fig. 8. The tenth percentile (B10) value is used to simplify this visualisation, which is provided in Table II alongside scale and shape parameters for each condition. The B10 PDIV values are all well above the rated isolation voltage of the modules of 4 kV (1 minute at 4 kV_{RMS}, 50 Hz AC). Increasing humidity caused a slight reduction in the sample PDIV, which was further reduced over time. This change was restored upon application of the dry-out condition. The negligible change in PDIV behaviour considering humidity for the gel encapsulated DBC substrates for this test can be more easily seen in the box chart shown in Fig. 9. These results show that the PDIV of the strong PD is not affected in any major way by changes in the ambient humidity.

TABLE II
SUMMARY OF WEIBULL STATISTICS FOR PD

Condition	Scale	Shape	B10 PDIV [V]
1: RH30-24h	4817	32.78	4542
2: RH85-24h	4742	28.95	4535
3: RH85-48h	4662	41.03	4460
4: RH30-24h	4738	29.77	4463

B. Time-Resolved Partial Discharge Study

Discharge amplitude is commonly used for qualification of systems using electrical insulation, often with a 10 pC threshold. Generally, a discharge with a greater amplitude corresponds to a greater degree of damage to the insulation for that event. The level of ambient humidity could impact discharge amplitude as absorbed moisture influences the composition of the system. Moisture absorption has been shown to increase the capacitance of silicone gel under similar conditions [27], and drastically reduces the breakdown voltage [14], indicating a severely reduced insulating performance. UHF amplitude has been linked to increasing discharge quantity in other insulation systems [28]. Therefore, this work uses the UHF amplitude associated with PD to infer the relative strength of a discharge event.

The time at which the PD event occurs relative to the rising edge of the test pulse is the PD time lag. This work uses the 10% value of the test pulse as a baseline for time lag estimations. Although for higher voltage pulses with faster slew rates, the approximate PDIV value should be reached sooner, PD may not always occur sooner. PD requires not only the inception voltage to be reached, but also that an initial electron is free to start avalanche, stimulated by field or thermionic emission. The barrier to field emission is reduced with increasing temperatures [29], but the impact of humidity in this case is not well understood.

Time-resolved PD (TRPD) analysis for silicone gel in [30] showed that discharges concentrated around the rising and falling edges of the test pulse, in line with much of the literature to date. To achieve a similar interpretation of the PD data recorded during PDIV determination testing, a holistic view of all PD events was considered. This is shown in Fig. 10. The behaviours of the strong and weak PD could then be compared.

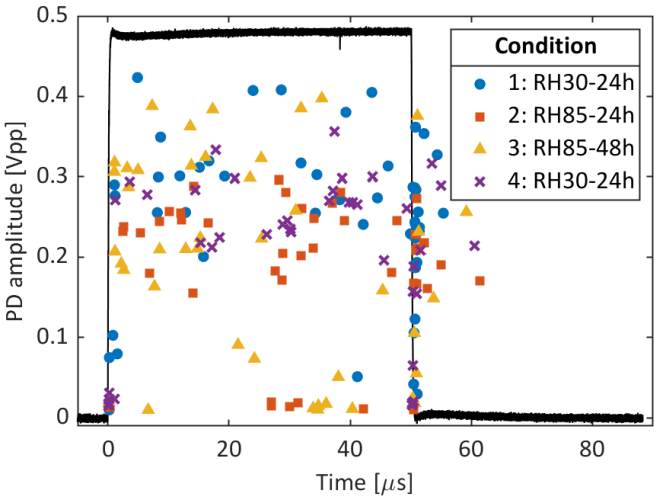

Fig. 10. TRPD visualisation of all PD events observed during PDIV determination testing, at each subsequent environmental condition. HV pulse shown for reference.

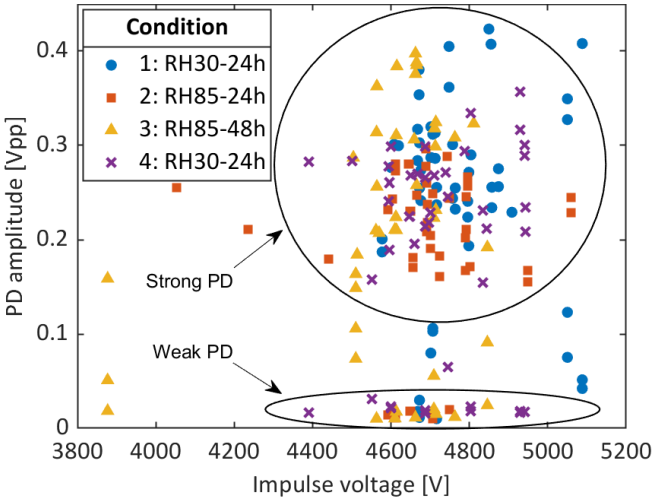

Fig. 11. Estimated UHF amplitude of all PD events observed during PDIV determination testing against impulse voltage at each subsequent environmental condition. Groupings of PD by amplitude highlight strong and weak PD.

To better capture the weak PD, the hardware HPF was reinforced with a steep digital HPF with the same cut-off frequency of 700 MHz. Although the commutation EMI was severely attenuated, the level of the noise floor was still sufficient to mask weak PD with amplitude less than 10 mVpp. PD events are spread along the test pulse, with a slight concentration at the falling edge. An increase in relative humidity does not impact the distribution of strong PD events in time. Fig. 11 shows PD amplitude against test voltage for each condition, revealing that increasing humidity only slightly reduces the mean strength of strong PDs, but this trend does not continue for a longer dwell in high humidity and the picture is not yet clear for weak PD. The humid environment caused several instances of significantly reduced PDIV, which was true of both strong and weak PD. The two groups are easily

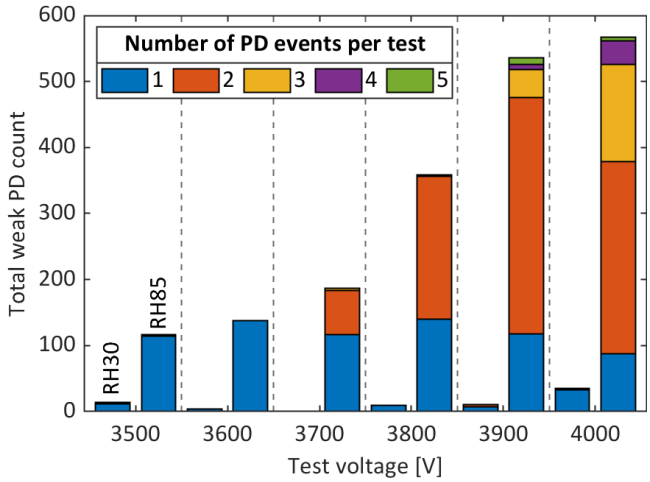

Fig. 12. Stacked bar chart of total weak PD count at each voltage. Left in groups is dry (30% RH) condition, right in groups is humid (85% RH) condition. Colouring of stacks inside bars represent the number of weak PD events observed in each singular test.

determined by their amplitude in Fig. 11. Strong PDs concentrate around 260 mVpp, while weak PDs concentrate around the detection threshold of 10 mVpp. The nature of these groupings is suspected to relate to the geometry of the samples and potential physical location of PD phenomena within them. A phenomenological explanation is proposed in Section V.

IV. Impact of Humidity Level on Weak PD

A. Influence of Humidity on Weak PD Count

The impact of ambient humidity and test voltage on the quantity of weak PD events is shown in Fig. 12. Each sample was subjected to 100 tests at each test voltage in each condition. Tests in the humid environment displayed a higher quantity of weak PD events overall, with the quantity further increasing with increasing test voltage. Multiple PDs are possible during a single test, originating from different locations on the sample or recurrence of PD within the same defect. Fig. 12 also shows the quantity of weak PDs per test per voltage at each environmental condition. A single weak PD event was the most common in the dry case, but humid tests presented higher weak PD counts more often as test voltage increases, indicating a more damaging PD regime.

B. TRPD of Weak PD

For time-resolved analysis of weak PD events irrespective of applied voltage, the PD lag taken from the standard deviation estimation technique was used to find the amplitude of weak PD in the recorded UHF waveform. The results provided in Fig. 13 provide an understanding of the impact of humidity on weak PD for the tested samples. Compared to the low humidity case, the high humidity environment had a larger proportion of higher amplitude events. This somewhat agrees with similar research on solid insulation [31], but the trend there is not clear. Consequently, the effect here is assumed to be due to the increased number of weak PDs in the humid case.

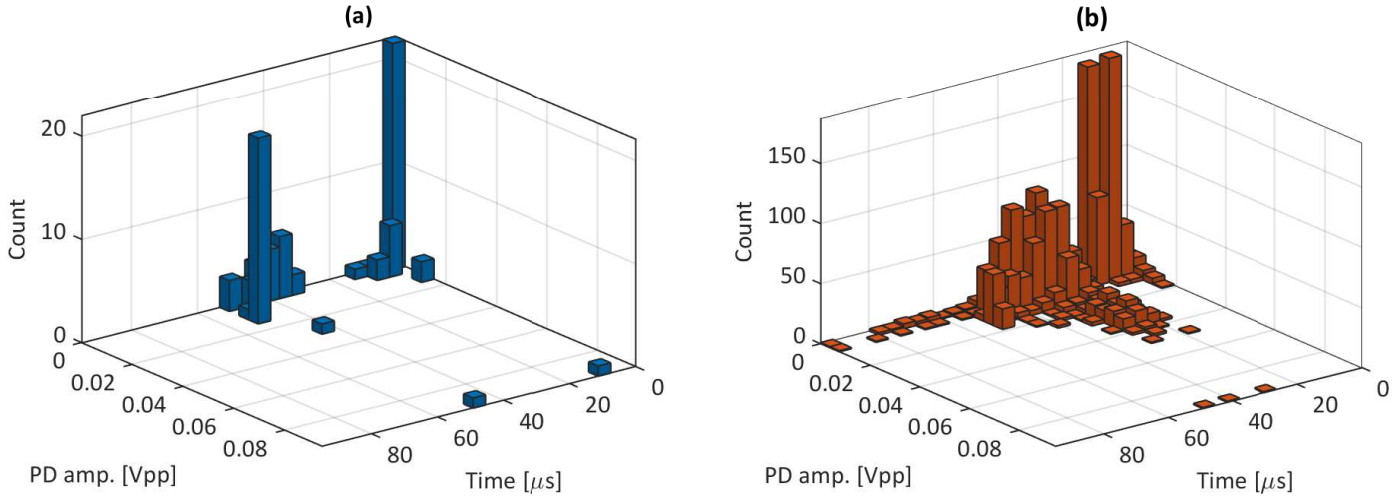

Fig. 13. Bivariate histograms of weak PD count against UHF amplitude and time lag of PD events. (a) 30% RH case, and (b) 85% RH case.

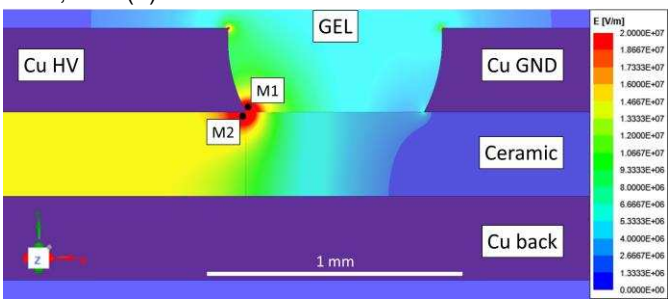

Fig. 14. Section of sample geometry in ANSYS Maxwell 2D for electrostatic simulation to determine E-field strengths near the triple junction at measurement points M1 and M2. Colour key scale is adjusted for emphasis.

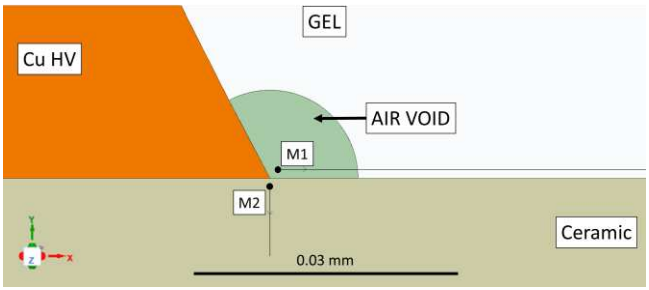

Fig. 15. Section of sample geometry in ANSYS Maxwell 2D for electrostatic simulation to determine influence of air-filled void at the triple junction on E-field strengths at points M1 and M2.

Higher amplitude events, concentrating around 50% of the pulse width (25 µs), were seen in high humidity. In the dry case, weak PD events concentrate around the commutation intervals (0 and 50 µs, Fig. 13(a)). With increased humidity, the distribution in time shifts to the rising edge and the centre of the test pulse (Fig. 13(b)). As UHF amplitude has been correlated to discharge quantity in [28], higher amplitude events are expected to cause more damage to the insulation, but more frequent low amplitude events are also expected to cause cumulative damage over time [32].

V. Suspected Origin of Strong and Weak PD

PD most commonly occurs at the triple junction of gel, ceramic, and copper due to the strength of the local electric field, which is enhanced on a microscopic scale by defects such as unfilled voids or sharp protrusions. Due to the lack of variation with humidity, strong PDs are attributed to voids within the ceramic at the triple junction, where the influence of absorbed moisture in the gel is limited. Weak PDs are shown to vary strongly with humidity and are attributed to voids within the gel at the triple junction. This PD category is expected to proceed primarily in the lateral direction and could cause irreparable damage to the insulation system over time via dissociative electron attachment (DEA) [32].

Two-dimensional electrostatic simulations were performed in ANSYS Maxwell using the same geometry of the test samples, with 4500 V excitation (close to mean of B10 PDIV values observed). The resultant E-field strength is shown in Fig. 14 to provide a qualitative illustration of the potential PD origin sites. Measurement points 1 µm away from the triple interface in the gel (M1) and in the ceramic (M2) are used to examine the maximum E-field strengths, following the approach of [33]. In that work, E-field strength is shown to be strongly correlated to PDIV and is hence determined to be a useful metric in determining PD susceptibility of insulation materials. Points M1 and M2 are chosen to correspond to weak and strong PD, respectively. The impact of absorbed humidity is simulated by adjusting the permittivity of the gel from 2.7 to 6, based on previous work [27]. The presence of an air-filled void is investigated in each case using assuming a spherical void of radius 1 µm in the gel bounded by the copper and ceramic; this geometry is shown in Fig. 15.

Simulated E-field strengths at M1 and M2 for each permutation of geometry and humidity are provided in Table III. Localised breakdown is expected to occur at lower voltages in the gel than in the ceramic, even when considering the difference in the E-field strengths. This indicates a lower PDIV for the gel, which agrees with the experimental results. The

TABLE III
2D ELECTROSTATIC SIMULATION E-FIELD RESULTS

Geometry	Condition	Gel permittivity	E-field strength [kV/mm]	
			M1	M2
No flaw	Dry	2.7	90.79	100.49
No flaw	Humid	6	70.71	82.13
Void	Dry	2.7	111.28	117.78
Void	Humid	6	100.53	108.90

statistics-based testing was performed at lower voltages and observed only weak PD. Higher voltages were used in the PDIV determination testing, which exhibited a mixture of strong and weak PD.

The E-field strength at M1 is always less than at M2, indicating that for a given voltage, PD within the gel should be weaker than within the ceramic. This agrees with the experimental results and is the key distinction between strong and weak PD. When moisture is absorbed by the gel, the E-field strength at both points is decreased, more so in the gel than the ceramic. Similar results are observed in [34]. PD amplitude is expected to reduce based on this result, but this is only somewhat reflected in the strong PD results and cannot be verified for weak PD. With an air-filled void at the triple junction, the E-field strength at both points is significantly increased. This highlights the well understood need for proper degassing techniques to eliminate voids. Additional work is required to fully discriminate between the two PD regimes and confirm their origin on the power module substrate to identify problematic regions which can be the focus of future material and geometry optimisation approaches.

VI. CONCLUSIONS

In this work, DBC rafts encapsulated in silicone gel are used to investigate PD characteristics when subjected to high slew rate unipolar square pulses, representative of field operation of modern power devices. Comparison is made of PDIV and TRPD results with samples in low humidity conditions (85 °C / 30% RH) versus high humidity (85 °C / 85% RH).

The amplitude of discharges recorded by UHF measurement implied two groupings unrelated to environmental condition and test voltage. Strong PDs are attributed to the ceramic between the top copper and bottom copper as they did not vary meaningfully with ambient humidity. The characteristics of weak PD varied strongly with ambient humidity and hence are attributed to the lateral gel-filled trench between top copper portions. For weak PD, testing was performed at fixed voltages to cope with their stochastic nature. The high humidity environment caused an increase in both the rate of occurrence and the amplitude of weak PD over the dry condition, with the alignment in time shifting away from the commutation intervals, concentrating near the rising edge and the centre of the test pulse.

Electrostatic simulation of representative sample geometries was performed, with the behaviour of the E-field strength at measurement points around the triple junction in the gel and the ceramic supported the strong and weak categorisation of PDs.

Weak PDs could cause irreparable damage through DEA within the silicone gel over time, occurring at lower voltages than strong PD. Traditional standards-based testing has long been shown to stress substrates in a non-representative manner and may not highlight a weakness in the insulation system in humid environments considering weak PD. The result could be the incorrect qualification of devices which are likely to degrade faster or fail early. This research indicates a need for standards which encompass the broad spectrum of degradation-causing stressors, in representative configurations.

ACKNOWLEDGEMENT

This work was funded by the Powertrain Research Hub (PTRH), a joint research partnership between the University of Sheffield, the University of Warwick, and the Offshore Renewable Energy Catapult. For the purpose of open access, the authors have applied a Creative Commons Attribution (CC BY) licence to any Author Accepted Manuscript version arising.

REFERENCES

[1] K. Fischer *et al.*, “Exploring the Causes of Power-Converter Failure in Wind Turbines based on Comprehensive Field-Data and Damage Analysis,” *Energies (Basel)*, vol. 12, no. 4, p. 593, 2019, doi: 10.3390/en12040593.

[2] A. J. Wileman, S. Aslam, and S. Perinpanayagam, “A road map for reliable power electronics for more electric aircraft,” *Prog. Aerosp. Sci.*, vol. 127, p. 100739, 2021, doi: https://doi.org/10.1016/j.paerosci.2021.100739.

[3] M. Borghei and M. Ghassemi, “Insulation Materials and Systems for More- and All-Electric Aircraft: A Review Identifying Challenges and Future Research Needs,” *IEEE Trans. Transp. Electrif.*, vol. 7, no. 3, pp. 1930–1953, 2021, doi: 10.1109/TTE.2021.3050269.

[4] D. J. Rogers, J. Bruford, A. Ristic-Smith, K. Ali, P. Palmer, and E. Shelton, “A Comparison of the Hard-Switching Performance of 650 V Power Transistors With Calorimetric Verification,” *IEEE Open J. Power Electron.*, vol. 4, pp. 764–775, 2023, doi: 10.1109/OJPEL.2023.3315348.

[5] W. Perdikakis, M. J. Scott, K. J. Yost, C. Kitzmiller, B. Hall, and K. A. Sheets, “Comparison of Si and SiC EMI and Efficiency in a Two-Level Aerospace Motor Drive Application,” *IEEE Trans. Transp. Electrif.*, vol. 6, no. 4, pp. 1401–1411, 2020, doi: 10.1109/TTE.2020.3010499.

[6] J. O. Gonzalez, R. Wu, S. Jahdi, and O. Alatise, “Performance and Reliability Review of 650 V and 900 V Silicon and SiC Devices: MOSFETs, Cascode JFETs and IGBTs,” *IEEE Trans. Ind. Electron.*, vol. 67, no. 9, pp. 7375–7385, 2020, doi: 10.1109/TIE.2019.2945299.

[7] P. Drexhage and S. Häuser, “SEMIKRON AN 16-001 - Effect of Humidity and Condensation on Power Electronics Systems,” 2022.

[8] M. T. Do, J.-L. Augé, and O. Lesaint, “Partial discharges in silicone gel in the temperature range 20-150°C,” in *2006 IEEE Conference on Electrical Insulation and Dielectric Phenomena*, 2006, pp. 590–593. doi: 10.1109/CEIDP.2006.312001.

[9] K.-W. Lee *et al.*, “Partial discharge characteristics of the ultra-high voltage cable insulators according to the measuring temperature,” in *2008 International Conference on Condition Monitoring and Diagnosis*, 2008, pp. 105–108. doi: 10.1109/CMD.2008.4580241.

[10] C. Hudon, M. Chaaban, M. Belec, and D. N. Nguyen, “Effect of temperature and thermal expansion on slot partial discharge activity,” in *2007 Electrical Insulation Conference and Electrical Manufacturing Expo*, 2007, pp. 122–126. doi: 10.1109/EEIC.2007.4562602.

[11] G. Finis, A. Claudi, and G. Malin, “Dielectric breakdown strength of silicone gel under various environmental conditions,” in *2005 IEEE Russia Power Tech*, 2005, pp. 1–6. doi: 10.1109/PTC.2005.4524423.

[12] G. Finis and A. Claudi, “On the Electric Breakdown Behavior of Silicone Gel at Interfaces,” *IEEE Trans. Dielectr. Electr. Insul.*, vol. 15, no. 2, pp. 366–373, 2008, doi: 10.1109/TDEI.2008.4483454.

[13] J.-L. Augé, O. Lesaint, and A. T. Vu Thi, “Partial discharges in ceramic

substrates embedded in liquids and gels," *IEEE Trans. Dielectr. Electr. Insul.*, vol. 20, no. 1, pp. 262–274, 2013, doi: 10.1109/TDEI.2013.6451366.
[14] G. Finis and A. Claudi, "On the dielectric breakdown behavior of silicone gel under various stress conditions," *IEEE Trans. Dielectr. Electr. Insul.*, vol. 14, no. 2, pp. 487–494, 2007, doi: 10.1109/TDEI.2007.344630.
[15] Y. Kikuchi *et al.*, "Effects of ambient humidity and temperature on partial discharge characteristics of conventional and nanocomposite enameled magnet wires," *IEEE Trans. Dielectr. Electr. Insul.*, vol. 15, no. 6, pp. 1617–1625, 2008, doi: 10.1109/TDEI.2008.4712665.
[16] Y. Kikuchi, T. Murata, N. Fukumoto, M. Nagata, Y. Wakimoto, and T. Yoshimitsu, "Investigation of partial discharge with twisted enameled wires in atmospheric humid air by optical emission spectroscopy," *IEEE Trans. Dielectr. Electr. Insul.*, vol. 17, no. 3, pp. 839–845, 2010, doi: 10.1109/TDEI.2010.5492257.
[17] M. Fenger and G. C. Stone, "Investigations into the effect of humidity on stator winding partial discharges," *IEEE Trans. Dielectr. Electr. Insul.*, vol. 12, no. 2, pp. 341–346, 2005, doi: 10.1109/TDEI.2005.1430402.
[18] T. Kaji, H. Asai, H. Kojima, and N. Hayakawa, "Combined Effect of Temperature and Humidity of Magnet-Wires on Partial Discharge Inception Voltage under Inverter-Surge Voltage," in *2018 IEEE Conference on Electrical Insulation and Dielectric Phenomena (CEIDP)*, IEEE, 2018, pp. 554–557. doi: 10.1109/CEIDP.2018.8544745.
[19] A. Rumi, A. Cavallini, and L. Lusuardi, "Combined Effects of Temperature and Humidity on the PDIV of Twisted Pairs," in *2020 IEEE 3rd International Conference on Dielectrics (ICD)*, 2020, pp. 906–909. doi: 10.1109/ICD46958.2020.9342030.
[20] N. Wang, I. Cotton, and K. Evans, "Impact of Thermal Cycling in Humid Environments on Power Electronic Modules," *IEEE Trans. Components, Packag. Manuf. Technol.*, vol. 2, no. 7, pp. 1085–1091, 2012, doi: 10.1109/TCPMT.2012.2195781.
[21] IEC, *61287-1 - Railway applications. Power converters installed on board rolling stock. Characteristics and test methods*. 2014.
[22] IEC, *60270+A1:2015 - High-voltage test techniques. Partial discharge measurements*. 2015.
[23] IEC, *61934 - Electrical insulating materials and systems - Electrical measurement of partial discharges (PD) under short rise time and repetitive voltage impulses*. 2011.
[24] S. S. Bugingo, P. Freere, K. Garde, H. Schalekamp, P. Ghimire, and R. Schultz, "Experimental Investigation of IGBT Silicone Gel Removal," in *2019 IEEE AFRICON*, 2019, pp. 1–4. doi: 10.1109/AFRICON46755.2019.9133966.
[25] Y. L. Ogundiran, A. Griffo, S. Sundeep, and J. Wang, "A Novel Embedded Sensor for Partial Discharge Detection in Inverter-Fed Machines," *IEEE Trans. Ind. Appl.*, vol. 58, no. 4, pp. 4698–4707, 2022, doi: 10.1109/TIA.2022.3177172.
[26] R. Ghosh, P. Seri, R. E. Hebner, and G. C. Montanari, "Noise Rejection and Detection of Partial Discharges under Repetitive Impulse Supply Voltage," *IEEE Trans. Ind. Electron.*, vol. 67, no. 5, pp. 4144–4151, May 2020, doi: 10.1109/TIE.2019.2921281.
[27] M. Sherriff, A. Griffo, C. Jia, and C. Ng, "Investigation of the impact of temperature and humidity on the capacitance of dielectric gel used for power electronics," in *11th International Conference on Power Electronics, Machines and Drives (PEMD 2022)*, 2022, pp. 91–96. doi: 10.1049/icp.2022.1023.
[28] Y. Jinggang *et al.*, "Research on the correlation between UHF signal energy and discharge quantity of partial discharge," in *2016 IEEE International Conference on High Voltage Engineering and Application (ICHVE)*, IEEE, 2016, pp. 1–4. doi: 10.1109/ICHVE.2016.7800798.
[29] Y. Ding, Y. Wang, H. Sun, and Y. Yin, "High-Temperature Partial Discharge Characteristics of Power Module Packaging Insulation Under Square Pulse With High Dv/Dt Based on Down-Mixing Method," *IEEE Trans. Ind. Electron.*, vol. 70, no. 7, pp. 7334–7342, 2023, doi: 10.1109/TIE.2022.3201276.
[30] X. Liu *et al.*, "Characteristics and Identification of Partial Discharge for Insulation Structures in High Voltage IGBT Modules Under Positive Square Wave Voltage," *IEEE Trans. Power Electron.*, vol. 38, no. 4, pp. 5347–5359, 2023, doi: 10.1109/TPEL.2022.3232327.
[31] P. Wang, Y. Li, A. Cavallini, J. Zhang, E. Xiang, and K. Wang, "The Influence of Relative Humidity on Partial Discharge and Endurance Features under Short Repetitive Impulsive Voltages," in *Annual Report - Conference on Electrical Insulation and Dielectric Phenomena, CEIDP*, IEEE, Oct. 2018, pp. 506–509. doi: 10.1109/CEIDP.2018.8544905.
[32] A. Rumi, J. G. Marinelli, D. Barater, A. Cavallini, and P. Seri, "The Challenges of Reliable Dielectrics in Modern Aerospace Applications: The Hazard of Corona Resistant Materials," *IEEE Trans. Transp. Electrif.*, vol. 8, no. 4, pp. 4646–4653, 2022, doi: 10.1109/TTE.2022.3191064.
[33] C. F. Bayer, U. Waltrich, A. Soueidan, E. Baer, and A. Schletz, "Partial discharges in ceramic substrates - Correlation of electric field strength simulations with phase resolved partial discharge measurements," in *2016 International Conference on Electronics Packaging, ICEP 2016*, The Japan Institute of Electronics Packaging, 2016, pp. 530–535. doi: 10.1109/ICEP.2016.7486884.
[34] L. Zhong *et al.*, "An Integrated Structure–Material Optimization Strategy for the Packaging of High-Voltage Insulated Gate Bipolar Transistors," *IEEE Trans. Dielectr. Electr. Insul.*, vol. 29, no. 6, pp. 2163–2170, 2022, doi: 10.1109/TDEI.2022.3211225.

Mark Sherriff (Student member, IEEE) received the Meng degree in electrical and electronic engineering from the University of Sheffield, Sheffield, U.K., in 2020.

He is currently pursuing a Ph.D. in electrical and electronic engineering with the University of Sheffield, Sheffield, U.K. His research interests include reliability of power converters, harsh environment degradation of power modules, and partial discharges in power modules.

Antonio Griffo (Member, IEEE) received the M.Sc. degree in electronic engineering and the Ph.D. degree in electrical engineering from the University of Napoli "Federico II," Naples, Italy, in 2003 and 2007, respectively.

From 2007 to 2013, he was a Research Associate at the University of Sheffield, Sheffield, U.K., and the University of Bristol, Bristol, U.K. He is currently a Professor of Power Electronics and Electric Drives with the Department of Electronic and Electrical Engineering, the University of Sheffield. His research interests include modelling, control, and condition monitoring of electric power systems, power electronics converters, and electrical motor drives for renewable energy, automotive, and aerospace applications.

Chunjiang Jia received the B.Sc. and M.Sc. degrees from Shandong University of Technology and Shandong University, Jinan, China, in 1999 and 2002, respectively, and the Ph.D. degree from the University of Birmingham, Birmingham, U.K., in 2008, all in electronic and electrical engineering.

He worked as a Research Associate with Manchester University, U.K., until 2011. He then joined Siemens wind power, Keele, U.K., as a Development Engineer. Since 2015, he has been working for Offshore Renewable Energy Catapult, Blyth, U.K., as a Senior Research Engineer, focusing on power conversion and reliability of wind turbine electrical infrastructure.

Chong Ng received the Ph.D. degree in electrical and electronics engineering from the University of Northumbria, Newcastle upon Tyne, U.K., in 2006.

He is currently the Head of Applied Research with Offshore Renewable Energy Catapult, Glasgow, U.K., and non-Exec Director of TUS-ORE Catapult Research Centre, Beijing, China. He and his team focus on offshore renewable energy technologies and novel test and validation solutions research and developments, with project portfolio in excess of £50 mil and is the named inventor on multiple international patents.

Zi-Qiang Zhu (Fellow, IEEE) received the B.Eng. and M.Sc. degrees in electrical engineering from Zhejiang University, Hangzhou, China, in 1982 and 1984, respectively, and the Ph.D. degree in electrical engineering from the University of Sheffield, Sheffield, U.K., in 1991.

Since 1988, he has been with the University of Sheffield, where since 2000, he has been a Professor with the Department of Electronic and Electrical Engineering. He is currently the Royal Academy of Engineering/Siemens Research Chair, and the Head of the Electrical Machines and Drives Research Group, the Academic Director of Sheffield Siemens Gamesa Renewable Energy Research Centre, the Director of CRRC Electric Drives Technology Research Centre, and the Director of Midea Electrical Machines and Control Systems Research Centres. His research interests include the design and control of permanent magnet machines and drives for applications ranging from electric vehicles through domestic appliance to renewable energy. Dr. Zhu was the recipient of the 2021 IEEE Nikola Tesla Award and the 2019 IEEE IAS Outstanding Achievement Award. He is a Fellow of the Royal Academy of Engineering, U.K.

David A. Stone received the B.Eng. degree in electronic engineering from the University of Sheffield, Sheffield, U.K., in 1984 and the Ph.D. degree in automatic weld penetration control from Liverpool University, Liverpool, U.K., in 1989.

After Ph.D., he joined the Electrical Machines and Drives Group, University of Sheffield, where he is currently a professor of electrical engineering. His research interests include battery management, energy storage and conversion, and energy utilization and power electronic applications, including dc–dc and motor drive systems.